

Distinguishing trivial and topological quadrupolar insulators by Wannier-Stark ladders

Alexander N. Poddubny^{1,*}

¹*Ioffe Institute, St. Petersburg 194021, Russia*

I study theoretically quadrupolar topological insulators under applied static electric field rotated along the crystal axis. I demonstrate, that the energy spectrum of this structure is a Wannier-Stark ladder that is quantized and directly distinguishes between the topological phase, possessing localized corner states, and the trivial phase, lacking the corner states. These results may find applications in the characterization of rapidly emerging higher-order topological phases of light and matter.

Introduction. Berry phase and Chern numbers are now well established concepts to characterize the excitations in crystalline solids [1]. Namely, depending on the value of the Chern numbers, calculated for bulk Bloch bands in infinite crystals, the finite samples, made from the same materials, will or will not have topological states propagating along their edges. Various interference techniques have been proposed to measure the Berry phase for Bloch bands, and the correspondence between bulk and edge features has been tested experimentally [2, 3].

Recently, a quadrupolar two-dimensional (2D) topological phase has been put forward [4]. Contrary to the traditional 2D topological insulators, the quadrupolar phase has localized corner states, rather than propagating 1D edge states. Such corner states have been demonstrated experimentally in the microwave [5], electric [6] and optical [7] setups. The topological nature of the structure is manifested by the fractional quantized corner charges and edge polarizations. The bulk topological feature is not exactly the Berry phase but the quantized phase of so-called nested Wilson loops calculated for the Bloch bands [4, 8]. The Wilson loops are significantly more complex entities than the Berry connection due to their inherently non-Abelian nature. Hence, the traditional interference techniques developed to measure the Berry phase [2, 3, 9] are inapplicable. The Wilson loop tomography has so far been developed only for the case of non-degenerate Bloch bands [10], while the quadrupolar phase has double-degenerate Bloch bands due to the reflection and chiral symmetries [8]. Hence, the fundamental question of measurable bulk manifestations of the quadrupolar topological phase remains open and a clear protocol to measure the topological invariants in the bulk is highly desired.

Here, I put forward a procedure for bulk spectroscopy of topological features of the quadrupolar phase based on the application of a constant electric field \mathbf{F} to the structure. The energy spectrum of the general one-dimensional biased periodic structure is a Wannier-Stark ladder of discrete levels [11–13]. The energy levels E_n of the ladder formed from a given Bloch band depend on the electric field as $E_n = E_n(F=0) + F(n+c)$, where $n = 0, \pm 1, \dots$ is the level number [14–16] and c are the Wannier center positions [17]. It is known for a 1D

Su-Schrieffer-Heeger structure [15] as well as for 2D and 3D topological insulators [14, 16, 18], that the centers $c = \{dE_n/dF_x\}$ contain information on the topological invariants ($\{x\}$ is the fractional part of x). Here, I extend this concept to the quadrupolar phase in a *rotated* electric field, $F_x \neq 0, F_y \neq 0$. I demonstrate, that the shifts $\{dE/dF_y\}$ are quantized for $F_x \neq 0$ and naturally reveal the topological phases of nested Wilson loops. This provides a transparent connection between the formal mathematical definition of the topological quadrupolar phase and its physical manifestations observable in the bulk.

Quadrupolar phase in the rotated electric field. The structure under consideration is schematically illustrated in Fig. 1(a) [8]. It can be described by a tight-binding Hamiltonian on a square lattice with the alternating intra-cell and inter-cell tunneling constants γ and λ (black and red solid lines). Dotted lines correspond to the couplings $-\gamma$ and $-\lambda$. Alternation of the positive and negative couplings ensures the non-zero π -flux through the unit cell, and opens the band gap in the energy spectrum of the infinite structure [4]. The momentum space

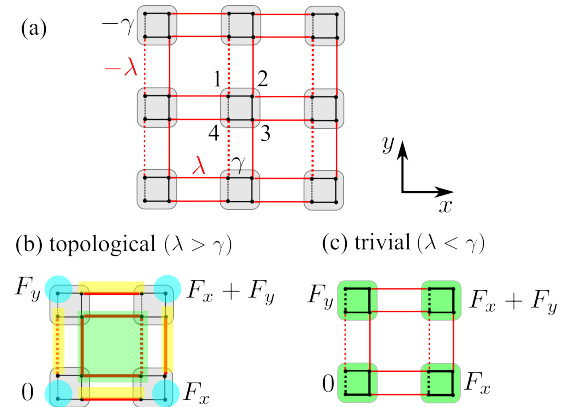


FIG. 1. Scheme of the structure under consideration. (a) Unbiased structure. (b,c) Biased topological (b) and trivial (c) structures. Green, blue and yellow shading depicts bulk, corner and edge states, respectively. External potential in the four unit cells is indicate on graph.

Hamiltonian for the periodic structure reads

$$H(k_x, k_y) = \begin{pmatrix} 0 & \gamma + \lambda e^{-ik_x} & 0 & -\gamma - \lambda e^{ik_y} \\ \gamma + \lambda e^{ik_x} & 0 & \gamma + \lambda e^{ik_y} & 0 \\ 0 & \gamma + \lambda e^{-ik_y} & 0 & \gamma + \lambda e^{ik_x} \\ -\gamma - \lambda e^{-ik_y} & 0 & \gamma + \lambda e^{-ik_x} & 0 \end{pmatrix}, \quad (1)$$

where \mathbf{k} is the Bloch wave vector and the basis corresponds to the atoms in the unit cell ordered as indicated in Fig. 1(a). Depending on the ratio between the couplings γ and λ , the structure can be either in topological, or in a trivial phase. Namely, for $|\gamma| < |\lambda|$ [Fig. 1(b)] it has corner states (blue circles) and edge states (yellow lines) in addition to the bulk states (green shading). In the opposite case, $|\gamma| > |\lambda|$ [Fig. 1(c)] the corner and edge states are absent. This is seemingly similar to the case of 1D SSH model, where the termination with a weak tunneling link leads to the formation of a zero-energy edge state [1]. However, the quadrupolar phase is qualitatively different from the 2D SSH lattice because of the presence of negative couplings that are essential for the formation of bulk band gap and topologically protected corner states, absent in a 2D SSH system [7].

The goal of this work is to distinguish between the topological and trivial phases from the bulk, rather than edge, spectral features by applying the external electric field \mathbf{F} . The main idea is sketched in Fig. 1(b,c). I assume that all four sites in each unit cell with the discrete coordinates $x, y = 0, \pm 1, \pm 2 \dots$ are biased by the energy $F_x x + F_y y$. In the trivial phase with $\gamma \gg \lambda$, [Fig. 1(c)], each Wannier state is fully located inside the given unit cell. The states have two-fold degeneracy and the energies $\pm\sqrt{2}\gamma$. The external potential does not split these states and only shifts them independently. In the topological phase with strong intra-cell couplings, $\lambda \gg \gamma$ the centers of the Wannier functions (green squares) are located between the unit cells [8], see Fig. 1(b). As such, each Wannier state is shared between four unit cells with different values of the external potential, and, contrary to the trivial case, the spectrum of the Wannier states will be split by the potential. Next, I prove this crude analysis by the rigorous calculation of the Wannier-Stark ladder.

Stark ladders for $F_y = 0$. I start by considering the structure with the electric field applied along the x direction and the periodic boundary conditions with the wave vector k_y along y . The energy spectra in the topological and trivial phases are shown in Fig. 2(a) and Fig. 2(b), respectively. The calculation demonstrates that the bulk Bloch bands are split due to the electric field and the two fans of levels, with the energies linear in electric field, emerge from each band. In the limit of $\gamma \ll \lambda$ ($\lambda \ll \gamma$) the energy levels are approximately given by the analyt-

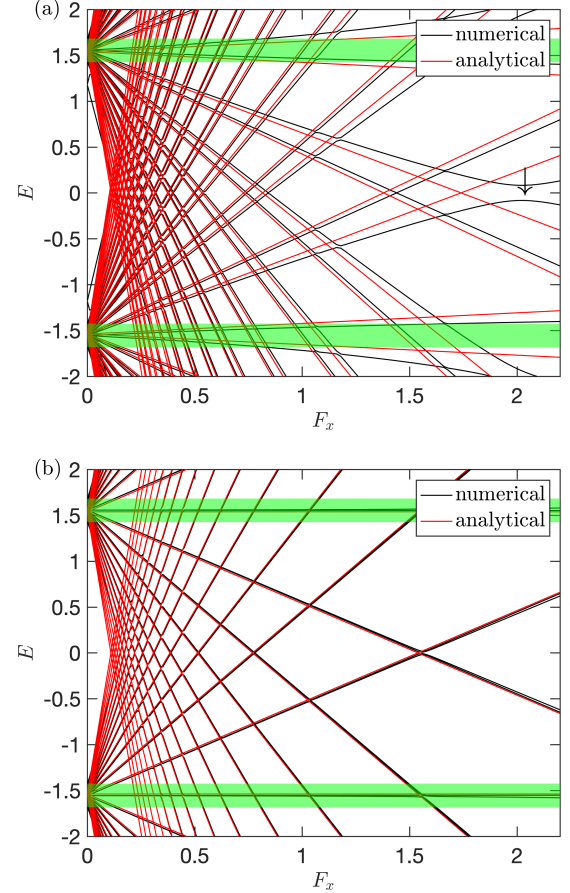


FIG. 2. Stark ladders depending on F_x calculated for $F_y = 0$. Panels (a) and (b) correspond to the topological ($\gamma = 0.2$, $\lambda = 1$) and trivial ($\gamma = 1$, $\lambda = 0.2$) structure. Black lines have been calculated numerically and red lines correspond to the analytical results Eq. (2), Eq. (3). Green shading shows the Bloch bands in the unbiased periodic structure. Vertical arrow in (a) indicates the splitting due to the Landau-Zener effect. Periodic boundary conditions with $k_y = 0.5$ have been used along the y direction, open boundary conditions with $N = 10$ unit cells have been used along x .

ical expressions

$$E_{n\sigma}^{(\text{topo})} \approx \sigma \left(\sqrt{2}\lambda + \frac{\gamma \cos k_y}{\sqrt{2}} \right) + F_x \left(n + \frac{1}{2} \pm \frac{\sqrt{2}}{4} q \right), \quad (2)$$

$$E_{n\sigma}^{(\text{triv})} \approx \sigma \left(\sqrt{2}\gamma + \frac{\lambda \cos k_y}{\sqrt{2}} \right) + n F_x, \quad (3)$$

where $n = 0, \pm 1 \dots$, $\sigma = \pm 1$ distinguishes the upper and lower bands and $q = 1 + \gamma \cos k_y / (2\lambda)$. These equations can be rigorously obtained as $E_{n\sigma} = F_x(n + c_{\pm})$, where $c_{\pm} = \ln(\lambda_{\pm})/2\pi i$ and λ are the eigenvalues of the 2×2 Wilson loop operator $W = \exp\{i/F_x \int_0^{2\pi} dk_x [E_{\sigma}(k_x) + iF_x u_{\sigma}^{\dagger} \partial u_{\sigma} / \partial k_x]\}$. Here $E_{\sigma} = \sigma\sqrt{2}\sqrt{\lambda^2 + \gamma^2 + \lambda\gamma(\cos k_x + \cos k_y)}$ are the Bloch band

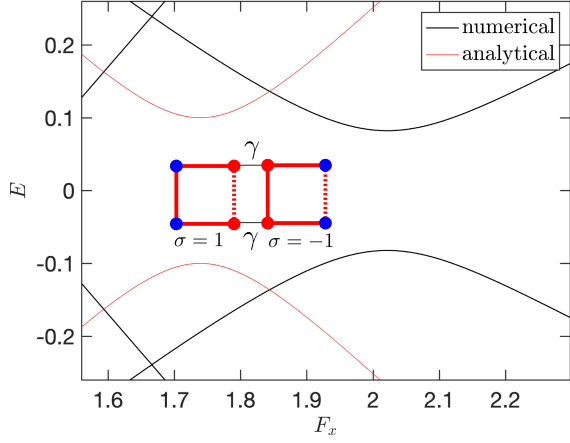


FIG. 3. Spectrum of the Wannier-Stark ladder from Fig. 2(a) enlarged in the vicinity of $F_x = 2$. Black lines show the results of numerical calculation, red lines show the analytical result Eq. (4). Inset schematically illustrates the spatial structure of the two Wannier functions of the coupled states, with red/blue circles corresponding to the values of $\psi(x, y) = \pm 1/2$.

energies and the 4×2 matrix $u_\sigma = [u_{1\sigma}, u_{2\sigma}]$ contains two Bloch functions u_1 and u_2 for the corresponding band σ [19]. The analytical answers Eqs. (2),(3) are shown by the red lines in Fig. 2 and well describe the numerical calculation. The difference between the topological and trivial cases is now clearly seen. In agreement with the naive explanation in Fig. 1(b,c), in the topological case the levels Eq. (2) are split by $\approx \sqrt{2}F_x/2$, while in the trivial case the states Eq. (3) remain almost twice degenerate.

Landau-Zener effect. Equations (2),(3) describe two independent Stark ladders formed from the two Bloch bands. However, it can be seen from Fig. 2(a), that in fact these ladders are not independent and feature avoided crossings. The largest anticrossing in Fig. 2(a) takes place at $F_x \approx 2$ and is indicated by an arrow. In Fig. 3 I have plotted the same levels in the larger scale around the field $F_x \approx 2$. Its physical origin can be understood by analyzing the two Wannier functions of the upper and lower bands ($\sigma = \pm 1$). Specifically, in the limit of $\lambda \gg \gamma$ the Wannier functions are fully localized on 4 sites between the unit cells [see Fig. 1(b)] with the absolute values of all four nonzero wavefunction components equal to $1/2$. The parameter n in Eq. (2) specifies the horizontal coordinate, i.e. the state n is located between the n -th and $n+1$ -th unit cells. Hence, for $F_x \approx 1.7\lambda$ one has $E_{1,-} \approx E_{0,+}$ which means that the Wannier states of upper and lower bands, shifted by one site, become degenerate (see the inset of Fig. 3). The tunneling between these states lifts the degeneracy and opens the gap with

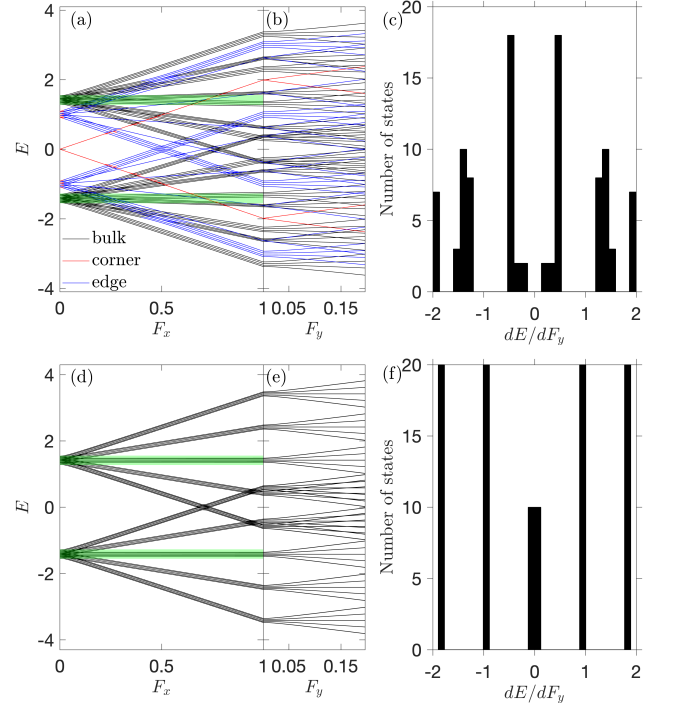


FIG. 4. Stark ladders for an open lattice with 5×5 unit cells depending on F_x (a,d) and F_y (b,e) in the topological (a,b,c) and trivial (d,e,f) phases with $\gamma = 0.15$, $\lambda = 1$ and $\gamma = 1$, $\lambda = 0.15$, respectively. Panels (c,f) show the distributions of dE/dF_y for $F_x = 1$, $F_y = 0.1$. Green shading indicates the Bloch bands in the unbiased periodic structure.

the width γ . Indeed, the analytical result [19]

$$\epsilon_{\pm} = \pm \frac{1}{2} \sqrt{(E_{1,-} - E_{0,+})^2 + \gamma^2}. \quad (4)$$

shown by the red lines in Fig. 3 well describes the exact numerical answer. The only difference is the small horizontal shift of the position of the anticrossing, that is a next order effect in the parameter F/λ , not taken into account in the approximation Eq. (2), Eq. (4). However, the width of the gap for the black curves in Fig. 3 is close to $\gamma = 0.2$ in agreement with Eq. (4).

Nested Wilson loops via the Stark ladders. It has been demonstrated in Fig. 2 that the application of the electric field modifies the structure in such way that its eigenstates become the Wannier functions, depending on the wave vector k_y . The phase of the nested Wilson loops proposed in Refs. [4, 8] is just the winding number of these functions calculated when k_y is varied across the Brillouin zone. I have verified numerically that this phase is equal to π (2π) for the topological (trivial) states in Fig. 2(a) [Fig. 2(b)] as expected [19]. Instead of the calculation of this phase under the periodic boundary conditions along the y direction one can consider a more realistic situation of a finite structure, open from all four sides. Application of an additional electric field along the y direction, corresponding to the rotation of the total electric

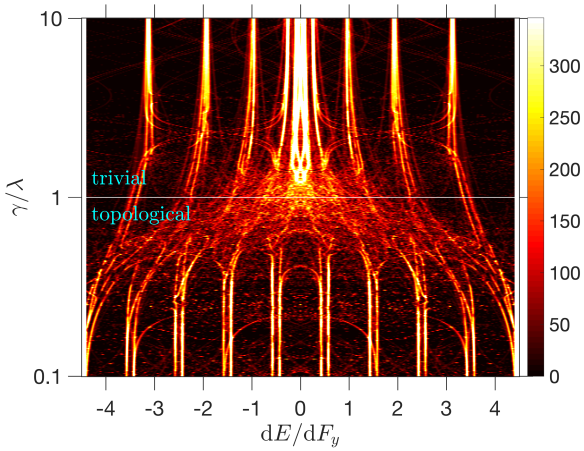


FIG. 5. Color map of the distribution dE/dF_y depending on γ for $\lambda = 1$, $F_x = 1$, $F_y = 0.1$. Calculation has been performed for the structure with 13×13 unit cells.

field, will then further split the states in Fig. 2. Next, I will demonstrate by an explicit numerical calculation, that the resulting *nested Stark ladder* is quantized and directly reflects the phases of the nested Wilson loops.

The results of the calculation are presented in Fig. 4. First, I apply the electric field along the x direction, which leads to the splitting of the Bloch bands for both topological [Fig. 4(a)] and trivial [Fig. 4(d)] structures, similarly to Fig. 2. Since now the topological structure is open in both directions, it also has edge and corner modes, indicated by blue and red colors, respectively, in addition to the bulk modes. The edge (corner) states have been formally defined as the states where the probability of localization at the sites at the edge (corner sites) is larger than 0.2. Application of an additional electric field along the y direction leads to the further splitting of the modes [Fig. 4(b,e)]. The key difference between the topological and trivial cases is the distribution of the derivatives dE/dF_y for given $F_x \neq 0$, shown in Fig. 4(d,f). In the topological structure this distribution has maxima around the *half-integer* values $\pm 1/2, \pm 3/2 \dots$, i.e. $\{dE/dF_y\} = 1/2$. In the trivial structure the distribution peaks are at the *integer* values $0, \pm 1, \pm 2 \dots$, i.e. $\{dE/dF_y\} = 0$. The broadening of the peaks, most distinct in the topological phase, is due to the finite size effects, that are relatively significant for the small structure with only 5×5 unit cells. This distinction between half-integer and integer values of the derivatives exactly corresponds to the difference between the π and 2π phase of the nested Wilson loops calculated in Ref. [4] for the topological and trivial structures. The advantage of the current construction with the Wannier-Stark ladders is that the topological phase arises naturally and can be accessible in finite open systems.

Finally, in Fig. 5 I calculate the variation of the distribution dE/dF_y for given fixed values of F_x and F_y

depending on the ratio γ/λ . Due to the larger size of the structure, more peaks are resolved as compared to Fig. 4. In order to simplify the presentation, the peak distribution has been convoluted with a Gaussian function with the dispersion of 0.02. In agreement with the results in Fig. 4, the positions of the peaks shift from half-integer to integer values with the increase of γ . This reflects the transition from the topological to the trivial regime.

To summarize, I have introduced the concept of bulk spectroscopy of topological invariants in the quadrupolar insulators by relating the quantized phases of nested Wilson loops to the spectra of Wannier-Stark ladders. The easiest experimental implementation of the current scheme might be provided by topoelectric circuits [6], where the on-site energies of individual sites can be tuned by introducing nonlinear elements [20]. These scheme can be directly generalized to other higher-order topological insulators [21]. Another potential avenue for future research, complementary to the study of discrete energy levels, is the analysis of the Bloch oscillations [16, 22] in the quadrupolar phase under rotated electric field.

I acknowledge the financial support by the Foundation for Advancement of Theoretical Physics and Mathematics “Basis” and the Russian Foundation for Basic Research Grants No. 18-29-20037 and 18-32-20065.

* poddubny@coherent.ioffe.ru

- [1] B. Bernevig and T. Hughes, *Topological Insulators and Topological Superconductors* (Princeton University Press, 2013).
- [2] M. Atala, M. Aidelsburger, J. T. Barreiro, D. Abanin, T. Kitagawa, E. Demler, and I. Bloch, “Direct measurement of the Zak phase in topological Bloch bands,” *Nature Physics* **9**, 795–800 (2013).
- [3] S. Mittal, S. Ganesan, J. Fan, A. Vaezi, and M. Hafezi, “Measurement of topological invariants in a 2D photonic system,” *Nature Photonics* (2016), 10.1038/nphoton.2016.10.
- [4] W. A. Benalcazar, B. A. Bernevig, and T. L. Hughes, “Quantized electric multipole insulators,” *Science* **357**, 61–66 (2017).
- [5] C. W. Peterson, W. A. Benalcazar, T. L. Hughes, and G. Bahl, “A quantized microwave quadrupole insulator with topologically protected corner states,” *Nature* **555**, 346–350 (2018).
- [6] S. Imhof, C. Berger, F. Bayer, J. Brehm, L. W. Molenkamp, T. Kiessling, F. Schindler, C. H. Lee, M. Greiter, T. Neupert, and R. Thomale, “Topoelectrical-circuit realization of topological corner modes,” *Nature Physics* **14**, 925–929 (2018).
- [7] S. Mittal, V. Vikram Orre, G. Zhu, M. A. Gorlach, A. Poddubny, and M. Hafezi, “Photonic quadrupole topological phases,” arXiv e-prints (2018).
- [8] W. A. Benalcazar, B. A. Bernevig, and T. L. Hughes, “Electric multipole moments, topological multipole moment pumping, and chiral hinge states in crystalline insulators,” *Phys. Rev. B* **96**, 245115 (2017).

- [9] A. V. Poshakinskiy, A. N. Poddubny, and M. Hafezi, “Phase spectroscopy of topological invariants in photonic crystals,” *Phys. Rev. A* **91**, 043830 (2015).
- [10] T. Li, L. Duca, M. Reitter, F. Grusdt, E. Demler, M. Endres, M. Schleier-Smith, I. Bloch, and U. Schneider, “Bloch state tomography using Wilson lines,” *Science* **352**, 1094–1097 (2016).
- [11] E. E. Mendez and G. Bastard, “Wannier-Stark ladders and Bloch oscillations in superlattices,” *Physics Today* **46**, 34–42 (1993).
- [12] S. Shevchenko, S. Ashhab, and F. Nori, “Landau–Zener–Stückelberg interferometry,” *Physics Reports* **492**, 1–30 (2010).
- [13] M. Glück, A. R. Kolovsky, and H. J. Korsch, “Wannier-Stark resonances in optical and semiconductor superlattices,” *Phys. Rep.* **366**, 103–182 (2002).
- [14] M. Taherinejad, K. F. Garrity, and D. Vanderbilt, “Wannier center sheets in topological insulators,” *Phys. Rev. B* **89**, 115102 (2014).
- [15] D. N. Maksimov, E. N. Bulgakov, and A. R. Kolovsky, “Wannier-Stark states in double-periodic lattices. I. One-dimensional lattices,” *Phys. Rev. A* **91**, 053631 (2015).
- [16] W.-R. Lee and K. Park, “Direct manifestation of topological order in the winding number of the wannier-stark ladder,” *Phys. Rev. B* **92**, 195144 (2015).
- [17] N. Marzari and D. Vanderbilt, “Maximally localized generalized Wannier functions for composite energy bands,” *Phys. Rev. B* **56**, 12847–12865 (1997).
- [18] A. R. Kolovsky, “Topological phase transitions in tilted optical lattices,” *Phys. Rev. A* **98**, 013603 (2018).
- [19] See Supplemental Materials for the details.
- [20] Y. Hadad, J. C. Soric, A. B. Khanikaev, and A. Alù, “Self-induced topological protection in nonlinear circuit arrays,” *Nature Electronics* **1**, 178–182 (2018).
- [21] F. Schindler, A. M. Cook, M. G. Vergniory, Z. Wang, S. S. P. Parkin, B. A. Bernevig, and T. Neupert, “Higher-order topological insulators,” *Science Advances* **4** (2018), 10.1126/sciadv.aat0346.
- [22] I. A. Dmitriev and R. A. Suris, “Damping of Bloch oscillations in quantum dot superlattices: A general approach,” *Semiconductors* **36**, 1364–1374 (2002).